European Journal of Molecular & Clinical Medicine
ISSN 2515-8260 Volume 07, Issue 02, 2020

COMPARISON ON AUGUMENTED DIAGNOSTIC METHODS FOR EARLY LUNG TUMOR

[1]J. Vijayaraj, [2,*]D. Loganathan

[1]Research Scholar, Department of Computer Science and Engineering, Pondicherry Engineering College, Puducherry, India
[2] Professor, Department of Computer Science and Engineering, Pondicherry Engineering College, Puducherry, India
[*]**Corresponding Author:** D. Loganathan, drloganathan@pec.edu**.in**

Abstract

Lung cancer is also the most serious illness of the day for smokers. Small cell lung cancer (SCLC) is the fatal type of lung cancer. This days, tumour detection is getting difficult. It is only in the final stage that this form of lung cancer can be detected. Computer assisted identification (CAD) and diagnosis mechanisms for lung cancer are an essential indicator of lung segmentation, as the execution of those mechanisms is based on the execution of computed tomography (CT) lung segmentation images. Image recognition system is commonly used for early identification and treatment. Lung cancer prediction, hereditary cell identification and environmental factors are essential factors in the development of lung cancer prevention strategies. By predicting the movement of tumour cell it will be easier to control the tumour spreading. This can be achieved to decrease the growth of the tumour cells using the motion prediction model. So this paper contrasts the methods used at the earlier level to identify lung tumors.

Keywords: Lung cancer, Computer aided detection, Segmentation, Computed tomography images, Prediction and early detection.

INTRODUCTION

Nearly 1,688,780 new cancer cases were analysed and around 589,430 deaths were caused, as indicated by the American Cancer Society. In 2015, about 13 percent of all recently analysed malignancies were lung tumours and about 27 percent of all cancer deaths in the United States were cases of lung cancer. Lung disease has been the world's largest cause of danger-related

transformations. One of the real reasons for the high lung tumour mortality rate is that lung malignancy is not expected to show clear symptoms before the disease progresses. Since metastatic cancer movement, approximately 85 percent of lung cancers are analysed, and subsequent therapy is not available. Lung disorders can be treated by early diagnosis and successful treatment. Early diagnosis of lung disorders increases the human survival rate by 15% to 18%[1]. In the beginning time lung diseases are shown in pneumonic nodules [2].

For visible imaging modalities for the examination and diagnosis of lung disorders, computer tomography (CT) is known as a standout technique. The other lung image processing requirement requires non-obtrusiveness, low cost and enhanced spatial determination. In this way, earlier pulmonary diagnosis and classification nodules are considered a powerful method of tumour detection.

Radiologists may characterise and risk lung pulmonary nodules with more tedious and subjective variables in clinical practise. Consequently, assessment plays a significant role in the successful diagnosis of disease development. Lung nodule classification is commonly regarded as a challenging task to approximate low difference, prediction of shape, variable size and erratic placement. Through implementation of supervised and unsupervised classification approach dangerous pulmonary nodules are estimated. Volume estimation and interpretation of 2D images is considered an important processing stage for lung image segmentation and classification. Segmenting lung images is the main step involved in lung image analysis. Segmentation is usually used as a set of steps involved in ROI-based computerised image processing. With the inclusion of noise, false data is generated in lung image segmentation, which imposes the requirement of precise lung segmentation[3]. The segmentation of the lung tumour is extremely heuristical in nature, incorporating trachea, delicate tissues, background artefacts, brochioles that display the characteristics of force and sores of malignancy.

Despite image processing, CT images provide tumour segmentation with effective lung image processing. Computer assisted detection (CAD) is currently used for tumour nodule segmentation[4]. The machine learning algorithm shows considerable success with efficient training data for successful lung tumour segmentation. On the other hand, with the inclusion of machine learning based calculation in the images, legitimate and adequate data is accessible at

any point. However, for 2D lung image segmentation, the Support Vector Machine (SVM)[5] provides an efficient processing system.

Most patients have severe, privately progressed or metastatic disease and their 5-year survival is approximately 1/14 of the beginning period. In this way, early diagnosis of pulmonary malicious nodules is urgent even than rehabilitation for dragging out life. To identify early pulmonary malignant nodule, CT is an enormous symptomatic strategy. To decrease the incidence of misdiagnosis, it has great affectability and flag to clamour ratio. Each of the CT scan cuts must be tested and screened for nodules to be identified, and radiologists mark the results as favourable or as a malignant candidate. Rehashing manual labour applies little attention and places relentless weight on them in order to dissect mass data and pick easily on the basis of analysis. [6]

To minimise the weight looked at by radiologists, various CADs[7] are scheduled and revised. The general CAD identification technique is split into 3 phases:

1) fragmentation of the lung region from the chest CT image; 2) identification of possible lung locale injuries; 3) using this calculation to diagnose diagnosed sores. Bunch of new methodologies for the exact lung district and division of small sores into 3 categories: model-based, threshold-based, and supervised methods of voxel classification. Multilevel threshold-based methodologies usually show signs of change in the above methods than active shape measurement and supervised methods of voxel classification[8]. Similarly, it has a conspicuous impediment to splitting the fuzzy sore, which is typically the logical malicious nodule technique, GGO (Ground Glass Opacity, for instance). Question as an important assignment of early identification of unknown nodules draws worldwide analyst considerations in the most recent two decades.

Because of the structure of cancer cells, prediction of lung cancer is the most difficult problem in which most cells overlap with each other. For precocious detection, the technique of image processing is commonly used for lung cancer detection, treatment and prevention. To detect lung cancer, various feature extraction and pattern recognition strategies are used. Lung cancer is defined as abnormal growth of cells that occur as a starting point in one or both lungs, mainly in the air passage line. Abnormal cells that are not capable of developing healthy lung tissue form

tumours. There is a rapid rise in lung cancer worldwide, with about 14 percent of newly diagnosed tumours being lung cancer by the American cancer society. Past studies have shown that cancer occurs mostly in patients at the age of 60 years[9].

The tumour can be benign or malignant. A benign tumour is one that is removed and stops spreading to other parts of the body. A malignant tumour develops quickly and expands to other areas of the body. Instead of using invasive procedures such as biopsy, medical imaging is chosen for looking inside the body since this approach is convenient and healthy for patients. Medical imaging plays a significant role in therapy and nodule detection. It is an important and precise technique for diagnosis.

LITERATURE SURVEY

An improved Random Forest (RF) estimate for classification of benign and hostile nodules was calculated by Li et al. ,[10] in thoracic processed tomography images. Firstly, improved random walk estimation was subsequently calculated, thereby segmenting pulmonary nodules. The strength, texture and geometric characteristics based on GLCM, pivot invariant uniform LBP and Gabor channel approaches have been combined in the discriminative feature vector generation here. General data has been used for the reduction of dimensionality. Benign and violent nodules have finally been developed with an updated RF classifier. Sensitivity of 0.92 and territories under the receiver-operating-characteristic (ROC) curve of 0.95 was realised by the characterization methodology indicated in the lung image consortium data collection. Yet, the cost of calculating this estimate was high.

A novel Structural Co-Occurrence Matrix (SCM) was explored by Rodrigues et al.[11] to deal with the tumour function in violent and benign tumour, in addition to harming it within some stages. Using the SCM system, the characteristics of tumour images were categorised into threatening or benign nodules by neglecting them.

The database consortium and image database asset operation databases provide data from the lung image for computed tomography investigation. Regarding nodule positions and their degrees of damage. Image calculation is based on grayscale and Housfield image consideration with Gaussian, Sobel and Laplace transformation consideration. The efficiency is measured on the basis of 96.7 percent separate characteristics for both F-Score and primary errand precision

measurements, and 53.2 percent F-Score and 74.5 percent accuracy in the second. The planning time for this proposal was high, be that as it may. In lung cancer, where 99.27 percent precision was obtained, successful genes.

Chen et al.[13] suggested NN ensemble-based CAD conspiring to classify pneumonic nodules that are amiable and threatening, which reached 0.79 ROC bend regions.

In addition, an analysis between ANNs and multivariable logistic regression (LR) for distinguishing dangerous nodules from benign knobs was conducted by Chen et al.[14]. ANNs had higher LR classification execution, and had a 95.5 percent ROC region and a 90.0 percent accuracy score.

Lin et al.[15] provides a collection of fractal-based features obtained from the Brownian fragmentary system of motion to distinguish dangerous from nice single pulmonary nodules. The classifier Support Vector Machine (SVM) was used to identify risks from benign nodules. It offers 0.8437 AUROC, 83.11 percent accuracy, 90.92 percent sensitivity, 71.70 percent precision, 80.05 percent positive and 87.52 percent statistical negative estimate. Han et al.[16] used both Gabor and LBP-based texture characteristics to establish 3D Haralick to identify nodules that are amiable as well as dangerous. Thinking of pulmonary nodules with a combined danger spectrum' 1 'and' 2 'as considerate and' 4 'and' 5 'as unsafe and using an SVM classifier obtained an AUROC of 0.94.

Thomas Pengo, Arrate Muñoz-Barrutía 2012, has created a multi-scale, multi-dimensional integrated CAD microscopy device that analyses and breaks down BAL experiments autonomously. This paper explains the product design and approves explicit protocols for image examination produced for this particular use. Bronchoscope-guided bronchoalveolar lavage (BAL) is an insignificantly obtrusive demonstrative technique that relies on patients' study and isolation of cells from bronchial epithelium that gives suspect lung masses on low-portion X-beam screening tomography images. Combined with the novel process of recoloration that consolidates lung immunopheno composition. The Cumulative Gray-Level Image (AGLI) method for gene definition was proposed by Abdelrahman and Abdelwahab[12]; here per gene base was taken from the aggregation number in the light of its request in the gene sequence and

then reflected in the picture region. To assemble exact and low-dimensional formulas for grouping hereditary shifts, AGLI is consolidated with 2D-PCA (Principle Component Analysis). The proposed measurement was linked with fluorescent in situ hybridization of genetic anomalous DNA loci on the best 10 malignant growth biomarkers. BAL guarantees a pioneering prior demonstrative instrument for lung carcinomas. In any event, the affectability of this procedure is highly dependent on the ability of the pathologist to accurately analyse a vast number of cells under the magnifying instrument over and over again. This is an extraordinarily focused work and error-inclined errand[17]

Vanessa H et al, direct pilot breath analysis using an artificial nose to classify theories that are significant contrasts between newly diagnosed LC patients as well as control subjects in scent print designs. The findings show guarantees that it has notable contrasts with lung malignant development compared and controlled subjects in subjects scent print. Further institutionalisation of the treatment will continue to boost the technique's affectability and accuracy, and the possibility to use different examination of ailments where signature labels appear in the breath. [18]

In 2016, Xuechen Li, LinlinShen * and SuhuaiLuo used stationary wavelet shift and convergence index channel to distinguish surface highlights and used AdaBoost to establish a white nodule-similarity outline. In order to determine the segregation level of applicants, a single variable was characterised. As a definitive measurement of lung nodule rivals, both disengagement degree and white nodule-resemblance are included. This methodology reveals favoured execution and vigour over those disclosed in previous studies. Over 80 percent and 93 percent of lung nodules in the lung region are separately differentiated in the JSRT database when false positives were 2 and 5 per picture. This technique has the potential to be used in clinical practise. [19]

Omar S. Al-Kadi suggested fractal study of time series constrast-enhanced (CE), CT images are used to identify non active and active malicious tumour. This approach seeks to increase the precision of CT tumour staging prediction by detecting malignant lung cancer violence. This technique offers an area of vascularized tumours with strong fractal features in which the branching of blood vessels is called a fractal operation. When 15 patients were injected with the contrast agent and at least 11 time series CE CT photographs of each patient were converted to the fractal dimension and the resulting lacunarity was calculated. The fractal texture

characteristics were averaged over the tumour area and the classification provided an accuracy of 83.3 percent[20].

Under the minimal invasive tumour ablative process, Ali SadeghiNaini et al, proposes a method for enhancing intraoperative ultrasound (US) image efficiency of deflated lung. US lung photographs are not sufficient and very low quality for image driven operation. In crushed lungs, these photos became very sensitive to oxygen. Good quality and accurate intraoperative lung images are required for fusion and tumour localization with real-time navigation data. This approach uses deflated lung computed topography image data, which is pre-operatively built, to enhance intraoperative US images. This improvement was achieved by using 2 registration processes. Improved US image output of collapsed lung focused and correctly located with preoperative CT counterpart is improved[21].

By using prevalent PET image contrast and spatial resolution of CT images, Wei Ju et al, effectively integrate two modalities. Random walk and graph cut strategy was combined to solve segmentation problems, where random walk was used as an initialization device to send object seeds on PET and CT images to graph cut segmentation. The problem of energy minimization is formulated by the problem of co-segmentation by the min cut / max flow process. A graph was generated with 2 subgraphs and a special relation where one is for PET and the other for CT. In order to separate tumour segmentation into 2 modalities, this special relation was used. The new method of energy representation is used to use the characteristics of PET and CT images. For Cat, 3D derivative costs and down-hill costs are suggested. Form penalty costs were combined into the energy feature for CT[22] to limit the number of tumour regions during segmentation.

Amjed S. Al-Fahoum, Eslam B. Jaber presents an automatic intelligent classification and identification of nodule structures. This technique is capable of showing the observed cancer scale, manually replacing radiologist method measurements, and measuring the distance of the cancer region length and width. For radiologists, the cancer detection area margin is a major challenge during diagnosis, and is an attribute that reflects tumour development. To simplify the identification of zone boundaries, each sensed area boundary that is used in observer variations is given by these methods. This system has the potential to show a histogram that helps radiologists to study cancer region homogeneity[23].

Tomas Krilavicius, IndreZliobaite, suggested an algorithmic approach to decide the 3D target location of each patient at the start of the procedure, aiming for a short set calibration period. Predictions of lung tumour movement is used to increase radiation therapy accuracy in order to correct for respiratory motion during radiation therapy, cough management or bean location. Exponential smoothing is considered and model parameters are fitted by minimising absolute disposition error and predicted signal fluctuations. Predictive success was measured on clinical datasets of diverse activities and a tested real-time prototype device of respiratory motion imitation[24].

Different facets of longitudinal modelling were studied by FatemehNasiri and Oscar Acosta-Tamayo. The overall aim was to refine a paradigm for new patients with the same condition on a given dataset from a particular longitudinal function derived from previous patients in a way that is worthy of generalisation. Lung cancer was the specific disease in this study, and the longitudinal features were tumour volume and a series of features based on tumour deformation over time. The distinction between the two groups was that the first-group patients survived therapy and decreased their tumour size substantially. We suggested a mixed-effect modelization scheme for the function modelling that allows each patient's modelization to benefit from both the patient-specific model and the patient-independent general model. The experiments showed that, relative to fixed-effect modelling, such modelling resulted in far higher prediction precision. [25]

Ivo Bukovsky, Noriyasu Homma, introduced the predictive approach for 3D lung tumour time series in real time series. As statistical techniques, the Quadratic neural model and MLP with one hidden layer were suggested and tested. This methodology has rules such as batch optimization for GD and Levenberg-Marquardt that are executed as methods of real time retraining. This approach was conducted for real time prediction and compared the predictive system capability and the 3D time series approach of the lung tumour.

QNU's supremacy over MLP offers real-time computational power, reproducibility and findings were concluded using the L-M and GD methods. For the precision estimation of 3DMAE of 1 mm for 1 second prediction horizon with less computational time than actual treatment time, findings from predictive models fulfilled this research[26].

COMPARISON OF EXISTING TECHNIQUES AND CONSOLIDATED BASED SURVEY

Table 1: Summary of common approaches of merits and demerits

AUTHORS	TECHNIQUES USED	ADVANTAGES	LIMITATIONS
Masahiko Aoki1*, Hiroyoshi Akimoto1, Mariko Sato1, Katsumi Hirose.(2016)	Dual energy computed tomography (DE-CT)	Significant correlation between SUVmax (maximum standardized uptake value) and AID (average iodine density). Based on FDG-PET/CT and DE-CT after high-dose SBRT, novel perspective on future development of local replace predictions.	Follow-up period was short, whether lc rates might reeduce with longerfollow-up, many factorsinfluence.
Carole Lartizien, Simon Marache-Francisco(2012)	Various methods of computer-aided detection (CADe) systems	Regarding very low contrast lesions, it significantly outperforms human sensitivity detection.	From normal cases, normal feature vectors are extracted whichare not available atclinics.

HongboZhua, Chun- Hyok Pak(2017)	In CT image, to segment lung region and suspected lung cancer lesion region, super pixel method is utilized.	Automatically diagnosis malignant nodules	Its accuracy is more than 89.5%.
Yang Song, WeidongCai, Jinman Kim(2012)	Regional lymph node disease and primary lung tumor analysis.	Automated system which gives robustand fast detection,time conservingmethod which gives 2nd opinion to physicians.	Abnormal lymph node and lung tumors separations aredifficult .PET gives highuptake activities areas and highlight non pathological areas.
ShuyinTaoa, b,*, WendeDongc , ZhihaiXu (2016)	For restoring blurred images by poisson noise, fast non-bind deconvolution method was utilized.	Compared with state- of-art method, this runs fast and restored image quality.	formulated by determining less negative logarithmic Poisson log-likelihood combined with TV

The table 1 given below presents the summary of various techniques used along with their benefits and limitations.

Table 2: Various techniques with limitations

AUTHOR	YEAR	TECHNIQUES USED	LIMITATIONS
Xuechen Li	2018	stationary wavelet Transform, convergence index filter	low visibility
Hongyang Jiang, He Ma*	2017	Significant CAD based automatic lung nodule system.	Must improve the detection precision
Yang Song*, WeidongCai,	2014	FDG PET-CT	Labeling performance is low
DijanaDjureinovic	2018	identified auto antibodies against CTAs	low in frequency of occurrence.
Wey Cheng Sim, Chet Hong Loh,	2018	Targeted next generation sequencing (TNGS)	lower in precision
Yanli Lin	2018	Plasma lncRNA signature	Not associated with histological types of lung cancer
YuhangWua,b, Hong Zhanga,b, Junfeng Xiang	2018	Novel Aptasensor	Lower accuracy level

Thomas Pengo, Arrate Muñoz-Barrutía	2012	Integrated Microscopy Computer-Aided detection platform	Lower stability
Vanessa H. Tran, Hiang Ping Chan	2010	Pilot breath analysis using an electronic Noise	Need improvement in accuracy
SayaliSatishKanitkar, N. D. Thombare	2015	Marker Controlled Watershed Transform	Edge detection needs more identification

Table 2 presents the techniques with their research limitations which motivated to begin this research.

OVERALL BLOCK DIAGRAM OF PROPOSED METHODOLOGY

The architecture of the proposed method is illustrated in figure 1 below.

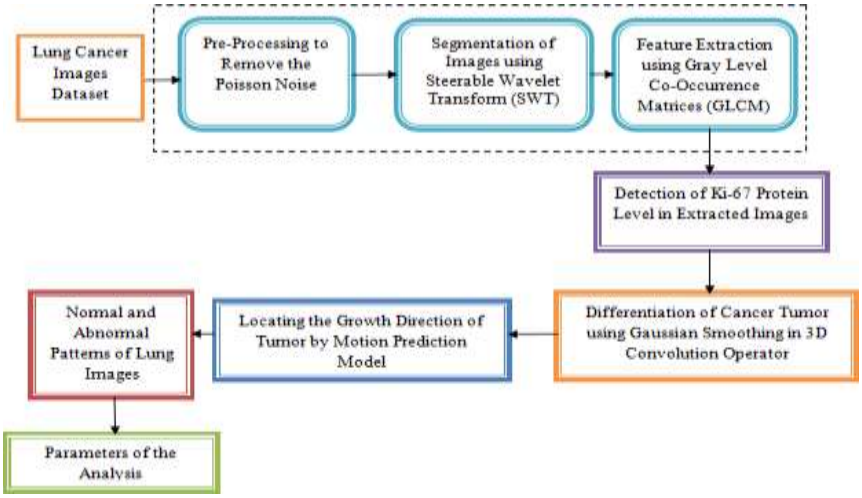

Figure.1: Overall architecture for proposed method

$$\hat{X}(\vec{\omega}) = \left\{ |H_0(\vec{\omega})|^2 + |L_0(\vec{\omega})|^2 \left(|L_1(\vec{\omega})|^2 + \sum_{k=0}^{n} |B_k(\vec{\omega})|^2 \right) \right\} X(\vec{\omega}) + a.t. \quad (1)$$

The dataset of lung images is pre-processed to eliminate the poisson noise, segmentation of images using Steerable Wavelet Transform (SWT) and extraction of features using GLCM. The amount of Ki-67 protein in the earlier symptoms of small cell lung cancer (SCLC) is observed in these pictures. Then the cancer tumour cells need to be separated, so Gaussian smoothing in the 3D convolution operator is used in the filtration process. The approach to find the path in the spread of the tumour goes after the recognition of the tumour cells, this can be achieved by motion prediction model. The findings display regular and irregular lung image patterns, and the values of the examined parameters are collected.

COMPARISON OF ALL THE PROPOSED MODULES

Steerable wavelet transform (SWT) and gray level co-occurrence matrices (GLCM):

Accurate segmentation of pneumonic nodules is a fundamental advance over the previous decade for consequent feature extraction segmentation strategies are established, how a free test remains to accurately section pneumonic nodules. Here, for good segmentation, the wavelet dependent steerable transformation scheme is proposed.

The steerable pyramid is the specific identification of multi-scale recursive shifts. In the Fourier field, where subbands are polar, disintegration is characterised.

Stage. Monstrous pulmonary nodule, but detachable. For example, n=1.{B k (almost k=0,1)} is a band pass-oriented philtre, H 0 (almost) is an unarranged high-pass channel, and L 1 (almost) is a low-pass narrowband channel. Two sections of the SWT conspire are combined,

such as decomposition and synthesis. In this, the image is at first exacerbated by the left half of the plan. The CT images are broken down into low-pass and high-pass classes with L 0 and H 0.0.0 steerable philtres.

The low pass band begins to split into a band pass subband structure B-0, ... ,B-N and low pass subband L-1. The low pass subband is subsampled by factor 2 along x and y bearings. The recursive structure is known by rehashing the shaded area to L i (i.e. scale of deterioration). At a related time , the right side of the graph gives part of the steerable wavelet plot to the mixture. The combined image is replicated by sampling the lower low pass subband by factor 2 and adding band pass subbands and high pass subbands arrangement. For i=1, recreation in the domain of frequency is:

That's where a.t. Linked words are shown. L-1 philtre should be obliged to zero reaction for frequencies greater than $\pi/2$ in both ω_x and ω_y to ensure the end of related terms, and the structure transition function should be equal to one bearing in mind the end objective of eliminating distortion of amplitude.

Extraction of functions using GLCM

The extraction of image features is a critical step in the PC-based framework. Extraction of features provides such criteria, depending on which decision is made by the PC system. The features can be acquired from it after the segmentation is done on the lung area, and the final control can be intended to differentiate nodules in the lung. In relation to the lung nodule, the whole portion that is calculated from the image passes on certain details. In defining the lung nodule as dangerous or non-harmful, this detail is highly helpful. The features isolated from the CT image can be used as demonstrative pointers[26] in this manner. Layer characteristics using co-occurrence matrix representation are the characteristics used as part of this inquiry. The GLCM is the 2nd factual structure process for removing texture characteristics. To begin with, the image is transformed into a l-grey-level image and GLCM is created by counting pairs of intensity occurrences between neighbour and current each pixels.

This approach creates feature vectors for each scale by using average matrices. Standardized GLCM is determined under the equation below:

$$G(i,j) = \frac{N(i,j)}{\sum_{m=0}^{l-1}\sum_{n=0}^{l-1} N(m,n)} \qquad (2)$$

Where, in the l-grey level chart, I and j are grey values. N(i, j)is the co-occurrence of the relative frequency of recurrence matrix by the following equation:

$$N(i,j) = \text{num}\,(\{[(x_1,y_1),(x_2,y_2)]\}|x_2 - x_1 = d\cos\theta, y_2 - y_1 = d\sin\theta, I(x_1,y_1) = i, I(x_2,y_2) \qquad (3)$$

Where (x_1, y_1) and (x_2, y_2) are positions of pixel

Ki-67 protein detection using the New Kaun Filter

The attribute removal of lung images using GLCM (Gray Level Co-Occurrence Matrices) is done only after the creation of the image to identify the cancer affected section. In order to locate the Ki- 67 protein, the kaunphiltre is then used for the filtration process. If normal cells have elevated protein levels of Ki-67, they are likely to transform into cancer cells. It helps to mask cancer cells in small cell lung cancer (SCLC) at the previous stage by identifying the dimension of Ki-67 protein in cells from the lung image dataset. As SCLC is highly normal for smoking, the signs of cancer at the previous stage are anything but difficult to detect. In order to prevent poison above, the lung CT image must be correct, and the kaunphiltre plan has been improved in this sense. This operates in the lung CT images without expelling edges or characteristics. Nonetheless, the noise is modified from multiplicative noise reveal to a photo showing subordinate applied material noise. The definition of the Mean Square Error (MSE) condition is related to the model for evaluating the key form of image from the beginning.

$$GL_{i,j} = \sum_{i=1}^{m=3,n=3}\sum_{j=1}^{m=3,n=3} Cp_{i,j} * W_{i,j} + M_{i,j} * (1 - W_{i,j}) \qquad 4)$$

Where (i,j) represents image pixels, (m , n) represents pixel information in rows and columns. In the philtre frame, Cp(i, j) is defined as a middle pixel M(i, j), which is referred to as a mean force approximation within the window, and W(i, j) is referred to as a weighting factor. When the noise is reduced, the noise execution is supposed to be based on this weight.

Gaussian 3D convolution operator:

In 3-D an isotropic Gaussian has form:

$$G(x,y,z) = \frac{1}{2\pi\sigma^2} e^{-\frac{x^2+y^2+z^2}{2\sigma^2}} \quad (5)$$

Gaussian smoothing implements 3D distribution as a point-spread function through the use of convolution. Discrete approximation to GF is produced before convolution results, as the image is stored as a set of discrete pixels. The Gaussian distribution is non-zero everywhere, which requires a large convolution kernel, but zero is terminated for more than 3 standard deviations. Gaussian with σ of 1.0.0. gives the sufficient integer-valued convolution kernel Gaussian value, which is not reliable since it differs non-linearly in pixels, may be used in the mask at the middle of pixels. Then integrate Gaussian with the value of an entire pixel. Integrals do not constitute integers. The array is rescaled so that Corners had value 1. Corners had value 1. The final sum of all mask values will be 273.

PNN Training Algorithm

Begin

initialize j = 0, n = pattern count

do j = j + 1

Normalize: $x_{jk} \leftarrow x_{jk}/(\sum_i^d x_{ji}^2)^{1/2}$

Train: $w_{jk} \leftarrow x_{jk}$

If $x \epsilon w_i$ then $a_{ic} \leftarrow 1$

Until j=n

end

Each pattern has to be placed in the input units to identify the X pattern. In addition, with the removal of the nonlinear function zk, each pattern must compute the inner product zk = wt x. Based on the associated group, each pattern unit contributes to the input likelihood for the image test function, taking into account the training-related Gaussian centre. The local approximation is based on local points with calculation concern, such as the discriminant gi(x) function with the Parzen window estimate with the underlying distribution function. The gi(x) limit provides the operating point for calculating the functional group.

COMPARISON OF THE PROPOSED TECHNIQUES

The study of different criteria used to test the efficiency of SWT and GLCM methods is shown in Table 3.

Table 3: Parametric Analysis for SWT and GLCM

Parameters	SWT	GLCM
Accuracy	87.2	86
Sensitivity	86	85
Specificity	90	89
Precision	98.5	97

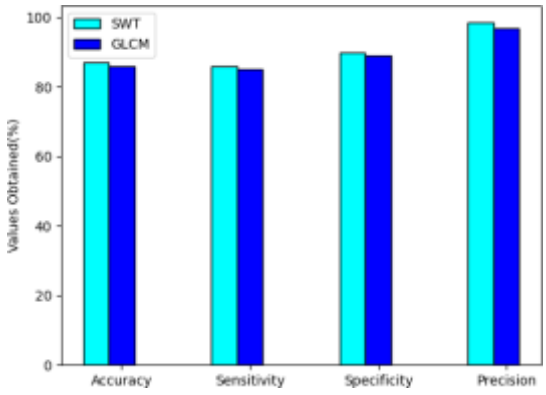

Figure.2: Comparison of Various Parameters for SWT and GLCM

A comparison of SWT and GLCM accuracy, sensitivity , specificity and precision is shown in Figure 2. The parameters used and the values obtained are represented by the X and Y axes. SWT and GLCM approaches are indicated by cyan and blue hue. It is noted that the SWT approach fits better relative to the GLCM method.

The values obtained for different parameters considered for testing the IKF method are presented in Table 4.

Table 4: Parametric Analysis for Improved Kaun Filter

Parameters	Accuracy	Specificity	Sensitivity	Precision
Image 1	99	98	99.6	96.5
Image 2	99.6	79.2	99.8	97
Image 3	97.4	97.3	98.5	97.5
Image 4	99.3	99.5	99.7	96.9

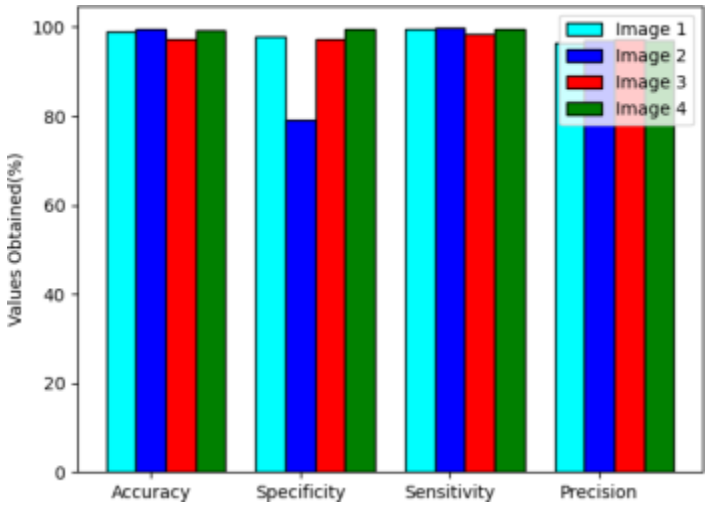

Figure.3: Comparison of Various parameters for 4 images

The comparison of Accuracy, Specificity , Sensitivity and Precision for the improved Kaun Filter system is shown in Figure 3. The parameters used and the values obtained are represented by the X and Y axes. Pictures 1, 2 , 3 and 4 are shown in Cyan, Blue, Red and Green respectively.

The values obtained for different parameters considered for testing the Gaussian 3D Convolution Operator method are presented in Table 5.

Table 5: Parametric Analysis for Gaussian 3D Convolution Operator

Parameters	Accuracy	Specificity	Sensitivity	Precision
Image 1	99.6	98	99.3	96
Image 2	98.5	97.3	98	99
Image 3	99.7	99.4	98	98
Image 4	99.7	99.4	98	98

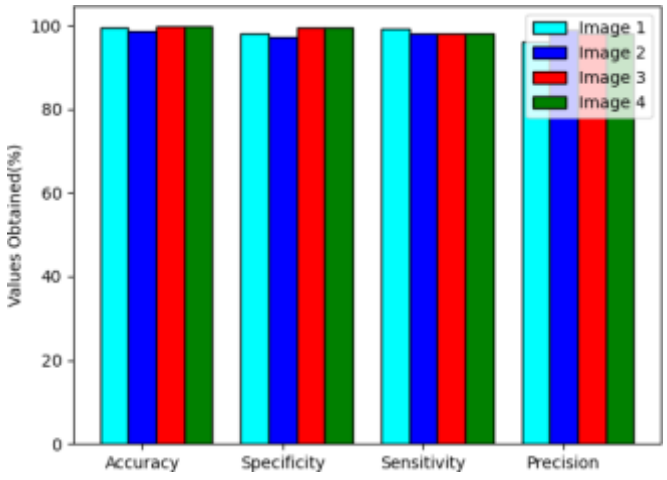

Figure.4: Comparison of Various parameters for 4 images

Figure 4 shows that the Gaussian 3D Convolution Operator approach contrasts precision, specificity , sensitivity and precision. The parameters used and the values obtained are

represented by the X and Y axes. Pictures 1, 2 , 3 and 4 are shown in Cyan, Blue, Red and Green respectively.

The values obtained for the different parameters considered for the evaluation of ANFN using the Probabilistic Neural Network (PNN) approach are presented in Table 6.

Table 6: Parametric Analysis for ANFN with PNN

Parameters	Accuracy	Specificity	Sensitivity	Precision
Image 1	91	91	96.5	90
Image 2	89	88	97	98
Image 3	96	97	97.5	95
Image 4	97	95	96.9	96

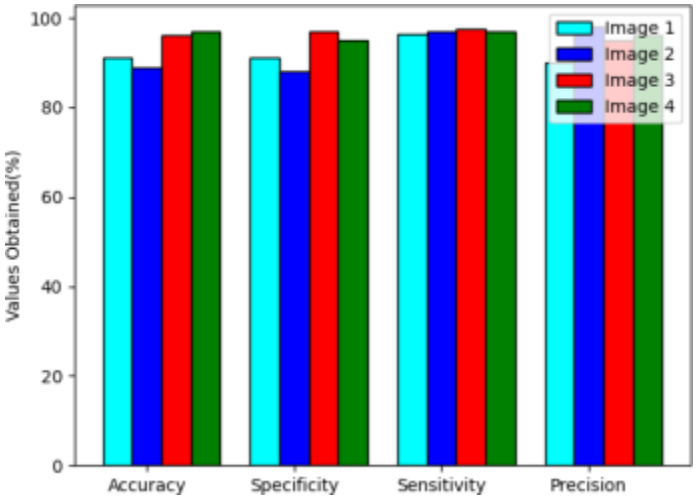

Figure.5: Comparison of Various parameters for 4 images

This comparison of the Probabilistic Neural Network (PNN) method's accuracy, specificity , sensitivity and precision is seen in Figure 5. The parameters used and the values obtained are

represented by the X and Y axes. Pictures 1, 2 , 3 and 4 are shown in Cyan, Blue, Red and Green respectively.

For the metrics considered for assessing different processes, Table 7 indicates the average results obtained.

Table 7: Parametric Analysis for Various Methods

Technique Used	Parametric Analysis			
	Accuracy	**Sensitivity**	**Specificity**	**Precision**
SWT and GLCM	87.2	86	90	98.5
IKF	98.8	93.5	99.4	96.9
Gaussian 3D Convolution Operator	99.3	98.5	98.3	97.7
ANFN with PNN	93.2	92.7	96.9	94.7

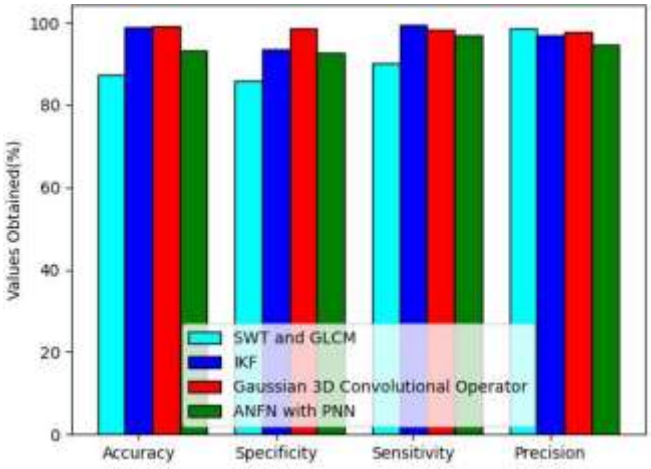

Figure.6: Comparison of Various Parameters for Various methods

This analysis of accuracy, specificity , sensitivity and precision for different methods is seen in Figure 6. The parameters used and the values obtained are represented by the X and Y axes. SWT, Enhanced Kaun Filter, Gaussian 3D convolutional operator and motion prediction model are respectively indicated by Cyan, Blue, Red and Green. It is observed from the above results that better output is given by the Gaussian 3D Convolutional operator.

CONCLUSION

This paper ends with the successful effects of the approaches suggested. Computer assisted identification (CAD) and diagnostic mechanisms for lung cancer are an imperative indicator of lung segmentation, as the application of these frameworks is focused on the implementation of lung segmentation in computed tomography (CT) pictures of the lungs. So this paper contrasts the methods used at the earlier level to identify lung tumours.

REFERENCES

1. Siegel R.L, Miller K.D, Jemal A, “Cancer statistics”, CA Cancer Journal of Clin., vol.65, pp.5-29, 2015.
2. Girvin F and Ko J.P, “Pulmonary nodules: detection, assessment, and CAD”, Am. J. Roentgenol, vol.191, pp.1057-1069,2008.
3. Mansoor A, “Segmentation and Image Analysis of Abnormal Lungs at CT: Current Approaches, Challenges, and Future Trends”, Radio Graphics,vol.35,no.4, pp. 1056-1076,2015.
4. Ranjeeth, S., Latchoumi, T. P., Paul, P. V. A Survey on Predictive Models of Learning Analytics. Procedia Computer Science, 2020;167, 37-46.
5. Gonzalez E.R and Ponomaryov V, “Automatic Lung nodule segmentation and classification in CT images based on SVM”, 9th International Kharkiv Symposium on Physics and Engineering of Microwaves, Millimeter and Submillimeter Waves (MSMW), pp.1-4,2016.
6. Xuechen Li, LinlinShen and SuhuaiLuo, “A Solitary Feature-based Lung Nodule Detection Approach for Chest X-Ray Radiographs”, DOI 10.1109/JBHI.2017.2661805, IEEE Journal of Biomedical and HealthInformatics.
7. Hongyang Jiang, He Ma, Wei Qian, MengdiGao and Yan Li, “An Automatic Detection System of Lung Nodule Based on Multi-Group Patch- Based Deep Learning Network”,

DOI 10.1109/JBHI.2017.2725903, IEEE Journal of Biomedical and HealthInformatics.

8. Yang Song, WeidongCai, Heng Huang and Xiaogang Wang, "Lesion Detection and Characterization With Context Driven Approximation in Thoracic FDG PET-CT Images of NSCLC Studies", IEEE Transactions On Medical Imaging, vol.33, no.2, 2014.
9. Latchoumi, T. P., Parthiban, L. Abnormality detection using weighed particle swarm optimization and smooth support vector machine.2017
10. Li X. X, Li B, Tian L. F and Zhang L, "Automatic benign and malignant classification of pulmonary nodules in thoracic computed tomography based on RF algorithm", IET Image Processing, vol.12, no.7, pp.1253-1264,2018.
11. Abdelrahman S. A and Abdelwahab M. M, "Accumulated grey-level image representation for classification of lung cancer genetic mutations employing 2D principlecomponent analysis", Electronics Letters, vol.54, no.4, pp.194-196, 2018.
12. Latchoumi, T. P., Sunitha, R. Multi agent systems in distributed datawarehousing. In 2010 International Conference on Computer and Communication Technology (ICCCT), 2010; 442-447, IEEE.
13. Chen H, Zhang J, Xu Y, "Performance comparison of artificial neural network and logistic regression model for differentiating lung nodules on CT scans", Expert Systems and Applications, vol.39, pp.11503-11509,2012.
14. Latchoumi, T. P., Ezhilarasi, T. P., Balamurugan, K. Bio-inspired weighed quantum particle swarm optimization and smooth support vector machine ensembles for identification of abnormalities in medical data. SN Applied Sciences, 2019;1(10), 1137.
15. Han F, Wang H, Zhang G, "Texture feature analysis for computer aided diagnosis on pulmonary nodules", Journal of Digital Imaging, vol.28, pp.99-115, 2015.
16. SayaliSatishKanitkar N. D, Thombare S. S. Lokhande, "Detection of Lung Cancer Using Marker- Controlled Watershed Transform", International Conference on Pervasive Computing(ICPC).
17. DijanaDjureinovic, Tea Dodig-Crnkovic, Cecilia Hellstr¨om, Georg Holgersson, Michael Bergqvist, Johanna S.M Mattsson, "Detection of autoantibodies against cancer-testis antigens in non- small cell lung cancer", S0169-5002(18)30571-3 DOI: https://doi.org/10.1016/j.lungcan.2018.09.012,2018.
18. Yanli Lin, QixinLeng, Min Zhan and Feng Jiang, "A plasma long noncoding RNA

signature for early detection of lung cancer", Translational Oncology, vol.11,no.5, pp.1225-1231,2018.

19. Omar S. Al-Kadi, "Texture Analysis of Aggressive and Nonaggressive Lung Tumor CE CT Images", IEEE Transactions on Biomedical Engineering, vol.55,no.7,2008.
20. Ali SadeghiNaini, Rajni V. Patel, and Abbas Samani, "CT-Enhanced Ultrasound Image of a Totally Deflated Lung for Image-Guided Minimally Invasive Tumor Ablative Procedures", IEEE Transactions On Biomedical Engineering, vol.57,no.10,2010.
21. Wei Ju#, Deihui Xiang#, Bin Zhang, Lirong Wang, "Random Walk and Graph Cut for Co- Segmentation of Lung Tumor on PET-CT Images", DOI 10.1109/TIP.2015.2488902, IEEE Transactions on ImageProcessing.
22. Amjed S. Al-Fahoum1 and Eslam B. Jaber, "Automated detection of lung cancer using statistical and morphological image processing techniques", Journal of Biomedical Graphics and Computing,vol.4, no.2,2014.
23. Tomas Krilavicius and IndreZliobaite, "Predicting respiratory motion for real-time tumor tracking in radiotherapy", arXiv: 1508.00749v1 [cs.AI], 2015.
24. FatemehNasiri and Oscar Acosta-Tamayo, "Mixed-Effect Modeling for Longitudinal Prediction of Cancer Tumor", arXiv: 1804.04590v1[stat.AP],2018.
25. Latchoumi, T. P., Balamurugan, K., Dinesh, K., &Ezhilarasi, T. P. (2019). Particle swarm optimization approach for waterjet cavitation peening. Measurement, 141, 184-189.